Volume 1 | Number 1 | Jan 2013 | Pages 1–100

Journal of
Materials Chemistry A

Materials for energy and sustainability
www.rsc.org/materialsA

ROYAL SOCIETY
OF CHEMISTRY

ROYAL SOCIETY
OF CHEMISTRY

www.rsc.org/materialsA

Journal Name

ARTICLE TYPE

MOFs-derived Porous Mn₂O₃ as High-performance Anode Material for Li-ion Battery

Zhongchao Bai,*[a] Yaohui Zhang,[a] Yuwen Zhang,[a] Chunli Guo,[a] Bin Tang[a] and Di Sun*[b]

MOFs-derived porous Mn₂O₃ are synthesized by a high-temperature calcination of a metal-organic framework, [Mn(Br₄-bdc)(4,4'-bpy)(H₂O)₂]ₙ (Br₄-bdc = tetrabromoterephthalate and 4,4'-bpy = 4,4'-bipyridine). The 10 porous Mn₂O₃ as an anode material for lithium ion batteries displays excellent performances, 705 mAh g⁻¹ after 250 cycles at 1 A g⁻¹.

Porous transition metal oxides have drawn enormous attention in a wide variety of energy and environmental applications such as 15 sewage treatment, catalysis, sensing, and energy collection, storage and conversion.[1] The common strategies for fabrication of porous transition metal oxides are always involved template (such as soft and hard template).[2] But their stringent experimental conditions and/or complicated post-treatment inevitably introduce 20 impurities and increase the cost, which make them unsuitable for large-scale production. Therefore, novel strategy is still necessary to develop in order to scaleably fabricate porous materials. The recently developed thermal decomposition method is considered to be a practical way to prepare porous materials because it only 25 needs a calcination process.[3-5] Contrasted with the template methods, this strategy is simple, cost effective, and more advantageous for large-scale production.[6] The porous structure has many advantages when used as electrode materials for energy storage, because of its high surface area (offer facile access of the 30 electrolyte to the electrode surface), nanosized feature (permit increased utilization of active material), and sufficient of voids (accommodate volume variation owing to first phase modifications during cycling.). Most recently, the exploration of Metal-Organic Frameworks (MOFs) as templates and/or 35 precursors to fabricate porous transition metal oxides materials presents great potential for applications in energy and environmental fields.[7-9] By a simple calcination at a high temperature, MOFs could completely convert to oxides, yielding many tiny pores inside the product. The prolific chemistry and 40 flexible structure of MOFs offer bountiful opportunities for us to fabricate porous structures, which makes them superior to other precursors.

Manganese oxide (Mn₂O₃) is of significant importance in technological applications including molecular adsorption, 45 biosensor, catalysis and energy storage, due to their structural flexibility and good physicochemical properties.[10-12] When used as electrode materials for Li-ion batteries, Mn₂O₃ will give higher energy density (compare to other transition metal oxides) because of the low voltage potential of manganese (average discharge 50 voltage at 0.5 V and charge voltage at 1.2 V). Therefore, it is considered as one of the most promising anode materials. The performance of the Mn₂O₃ anode, however, has been frustrated by its poor electrochemical reactivity and large volume changes during the lithium intercalation/deintercalation.[12] To solve these 55 issues, various nanostructured Mn₂O₃ anode materials have been fabricated to achieve improved electrochemical performance.[13-15] Despite remarkable progress, the Mn₂O₃ electrodes are still far from commercialization. Therefore, new strategies for constructing advanced Mn₂O₃ electrodes with high power rates 60 and long cyclic stability are still needed. It is well known that electrode materials with appropriate porous structures cannot only increase their energy density, but also ameliorate their rate capabilities. Thus, the porous Mn₂O₃ may have a bright future as the high performance anode materials for LIBs. To date, only a 65 few Mn₂O₃ porous structures have been synthesized; however, these compounds have represented enhanced electrochemical performances including high capacity, good cycling stability, and rate capability as anode materials for LIBs.[13-17]
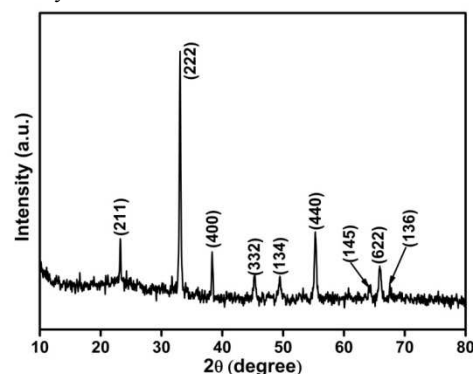
70 **Fig. 1** the XRD patterns of the product obtained after the calcinations.

In this communication, we report a facile strategy to fabricate Mn₂O₃ porous structures derived from a MOFs. Because of its easy preparation, high yield, and low cost, [Mn(Br₄-bdc)(4,4'-75 bpy)(H₂O)₂]ₙ (Mn-LCP, Br₄-bdc = tetrabromoterephthalate and 4,4'-bpy = 4,4'-bipyridine) was selected as the precursor to synthesize porous Mn₂O₃.[18,19] First, Mn-LCP was synthesized
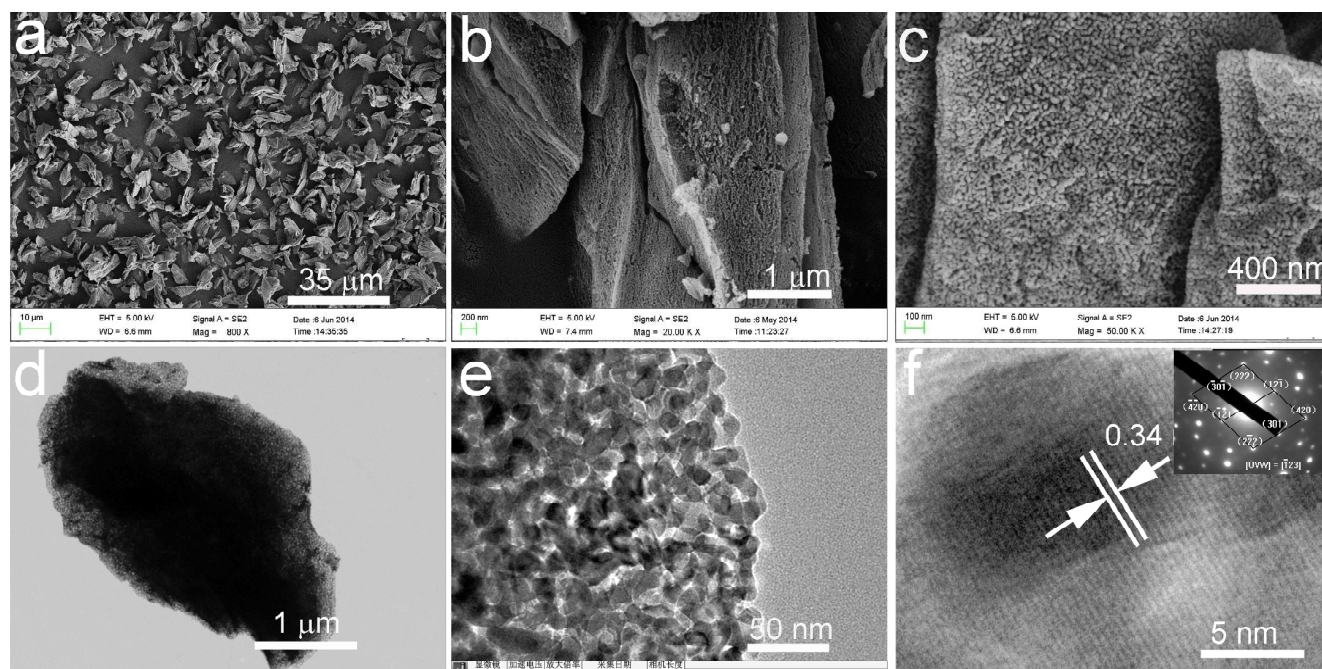
Fig. 2 (a) Low, (b) high-magnification, and (c) cross-sectional SEM images of the 3D porous Mn_2O_3; (d) low, (e) high-magnification TEM and (f)

HRTEM images of the synthesized 3D porous Mn_2O_3.

from manganese (II) nitrate hexahydrate, 2,3,5,6-
tetrabromoterephthalic acid, NaOH, and 4,4'-bipyridine at room
temperature. Then, the precipitate was collected and calcined at
600 °C for 2 h to obtain the porous Mn_2O_3. Due to its excellent
geometry, the porous Mn_2O_3 displays improved electrochemical
performance including high specific capacity, long cycling
stability and good rate property.
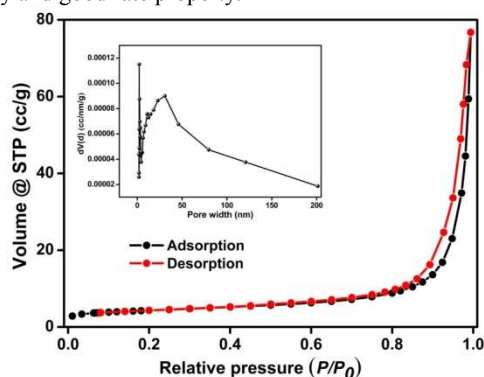
Fig. 3 N_2 adsorption/desorption isotherm of porous Mn_2O_3 at 77 K and
their pore size distribution curve (inset).

Mn-LCP, is the intermediate for the final product of porous
Mn_2O_3, examined by the XRD patterns and shown in Figure S1.
All the diffractions match well with the standard patterns of the
Mn-LCP. After the high temperature calcinations, Mn-LCP was
completely converted to Mn_2O_3 along with the release of gases
(Figure 1). All the reflections of XRD patterns are agreement
with the cubic structure (space group $Ia\bar{3}$) of Mn_2O_3 (JCPDS
card no. JCPDF 65-7467). This process is supported by the TGA
curve. Although the decomposition of Mn-LCP in air starts at 300
°C (Fig. S3), the calcination temperature in our case is set at 600
°C to guarantee the complete conversion. The release of gases

from the decomposition of Mn-LCP makes the product highly
porous, which favors the tolerance of active materials to volume
variations and boosts the structure stability.

The morphology and structure features of the produced porous
Mn_2O_3 are characterized by SEM and TEM techniques. The
panoramic view of the product is presented in Figure 2a, where
one can see that the sample is made up of microcrystals with size
of ~5 μm. Close-up observations reveal that the microcrystals
composed of many tiny particles which assembled up to 3D
porous structure (Figure 2b and c). A typical cross-section of the
porous Mn_2O_3 is presented in Figure 2c, in which the porous
structure can be further fixed by the evident holes. Besides, the
nanosized building blocks can be also clearly disclosed. Such a
fascinating porous structure is thought advantageous in
accommodating the strain derived from the Li^+
insertion/extraction, and accessing of the electrolyte to the
electrode surface.[16] Therefore, the improved electrochemical
performances including cycling performance and rate
performance might be obtained. The porous feature is also
supported by distinct contrast in the TEM image (Figure 2d)
though the particle size is big. The magnified TEM image
disclosed that the second particle size of the sample is about 10
nm and they interconnected each other to produce 3D porous
structure. A representative HRTEM image of porous Mn_2O_3 is
shown in Fig. 2f. The interplanar distance is 0.34 nm, which
agrees with (220) plane of cubic Mn_2O_3. The selected-area
electron diffraction (SAED) pattern (in set Figure 2f) taken from
the entire porous Mn_2O_3 clearly shows a single-crystalline
structure.

The porous feature of the prepared porous Mn_2O_3 was further
investigated by nitrogen adsorption-desorption instruments and
displayed in Fig. 3. The sample demonstrates isotherm of type □
which (Fig. 3) indicates it has large porosity.[11, 12] The Mn_2O_3

sample shows a high surface area of 15.34 $m^2 g^{-1}$ and total pore volume of 0.118 $cm^3 g^{-1}$. The pore size distribution evaluated from adsorption isotherms is represented in Fig. 3 (the inserted curve). The large surface area and porous framework of the as-
5 synthesized Mn_2O_3 make it potentially favorable for applications
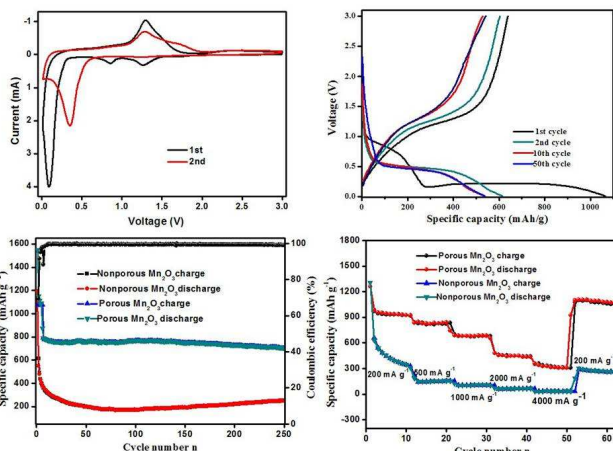
Fig. 4 (a) Cyclic voltammograms of the obtained Mn_2O_3 in the voltage range of 0.01-3.0V at a scan rate 0.1 mV s^{-1}; (b) The 1st, 2nd, 10th and 30th voltage profiles of the porous Mn_2O_3 electrode between 0.01 and 3 V
10 at the current density of 1000 mA g^{-1}. Galvanostatic discharge-charge cycling was performed in the voltage range from 0.01 to 3.0 V. (b) Compared cycling performance and coulombic efficiency versus cycle number of porous Mn_2O_3 and microsized Mn_2O_3 electrode at a current density of 1000 mA g^{-1}. (c) Rate capabilities with increasing current
15 density of the porous Mn_2O_3 and microsized Mn_2O_3 electrode.

such as electrochemical supercapacitor and high performance LIBs, since they can favor the ion transfer at the electrode/electrolyte interface.
20   When used as an anode material for LIBs, the porous Mn_2O_3 exhibits outstanding lithium storage performance. The good cycling stability of the porous Mn_2O_3 is affirmed by cyclic voltammetric examinations, and displayed in Fig. 4a. In the first cathodic scan, three reduction peaks are observed. The first one
25 centers at 1.25 V, which can be ascribed to the lithiation of Mn^{3+} to Mn^{2+}.[12] The second one (0.95 V) may come from the formation a solid electrolyte interphase (SEI) layer on the electrode surface.[5] The insensitive peak at low voltage (0.2 V) is attributable to the reduction of Mn^{2+} into metallic Mn nanoparticles along with the
30 formation of Li_2O matrix. In the subsequent anodic process, one peak locating at around 1.28 V is detected, which is derived from the oxidation of metal Mn^0 to MnO and the decomposition of Li_2O.[20,21] In the second cycle, the initial two reduction peaks (1.25 and 0.95 V) in the first cycle disappears, while the last one
35 shifts to 0.36 V. This circumstance is common in transition metal oxides because some side reactions and structure arrangements only occurred in the first cycle.[16] The anode process of the second cycle is very similar to the first cycle except for a decrease in the intensity, which implies irreversible capacity of the porous
40 Mn_2O_3 electrode. In the following cycles, the CV curves are similar to the second cycle and almost overlapped, indicating the good electrochemical reversibility of the porous Mn_2O_3.
    Fig. 4b exhibits the 1st, 2nd , 10th and 50th charge/discharge curves of the porous Mn_2O_3 at a current density of 500 mA g^{-1}.

45 The voltage is dropped to a plateau ca. 0.26 V from the open circuit potential followed by decreased slowly to 0.01 V, accounting for the reduction of Mn^{2+} to Mn^0 (in the first cycle). [12] The initial discharge and charge capacities of the porous Mn_2O_3 is 1158 mAh g^{-1} and 852 mAh g^{-1}, respectively, corresponding to
50 an initial coulombic efficiency of 74%. The low initial coulombic efficiency may be mainly attributed to the irreversible processes such as the formation of a SEI layer and electrolyte decomposition.[23] In the second discharge process, the plateau changes to about 0.5 V due to the drastic lithium driven and
55 activation of the electrode.[12] After then, the profiles do not change much. This result is agreement well with the CV examination.
    Fig. 4c shows the cyclic performance and coulombic efficiency versus cycle number of porous Mn_2O_3 at a current density of
60 1000 mA g^{-1}. Fast capacity decay in the first cycles is observed, due to the complicated side-reactions and irreversible structure transformation. Afterward, the capacity was generally maintained because the electrochemically reversible structures for Li-ion insertion reaction have been established. After 250 cycles, the
65 porous Mn_2O_3 still maintains a high discharge specific capacity of 705 mAh g^{-1}. For comparison, the microsized Mn_2O_3 were synthesized and its electrochemical properties were tested in the same situation (Fig. S2). Only after a few cycles, the specific capacity dropped to about 200 mAh g^{-1} (Fig. 4c). The mainly
70 reason for this result may be that the porous structure provides large surface area for the effective contact of the electrode and electrolyte, and plenty of void spaces for accommodating the huge volume variations during lithium uptake/release. [22,23] In the microsized Mn_2O_3, the large volume variations lead to
75 pulverization of the electrode and then bad cyclic stability. Furthermore, the electrochemical property is also better than most of the former reports of the Mn_2O_3 materials, such as mesoporous straw-sheaf-shaped and oval-shaped Mn_2O_3 delivered capacities of 380 mA h g^{-1} and 320 mA h g^{-1} in the 150th cycle at the
80 current density of 200 mA g^{-1}, respectively.[10] Mn_2O_3 sheets exhibited 521 mA h g^{-1} at the current density of 300 mA g^{-1}.[11] Porous Mn_2O_3 nanofibers, nanorods and nanowires are maintained at 404, 384 and 374 mAh g^{-1} after 10 cycles at the current density of 100 mA g^{-1}.[13] Porous Mn_2O_3 microsphere
85 displayed 600 mA h g^{-1} at the current density of 1200 mA g^{-1}.[15] The coulombic efficiency of the porous Mn_2O_3 is calculated about 73.7% in the first cycle, while it increases to about 99% in the second cycle and retains at this value for the whole test process.
90   The compared rate performance for the prepared microsized and porous Mn_2O_3 are displayed in Fig. 3d. As the current densities changes from 200 to 4000 mA g^{-1}, the specific capacities of 917, 880, 756, 572 and 450 mAh g^{-1} are correspondingly obtained for porous Mn_2O_3. More significantly,
95 when current density restores to 200 mA g^{-1}, the capacity of the electrode also recovers to 950 mAh g^{-1}. This result indicates that the porous Mn_2O_3 structure is stable in various current densities. Accordingly, the contrasted microsized Mn_2O_3 exhibits average capacities of 450, 147, 105, 62 and 33 mAh g^{-1}. With the current
100 density increasing, the capacity of microsized Mn_2O_3 sharply declines because at the high current density, the polarization of the electrode is became more severely. The porous structure has many voids which is similar to reducing the particle size, decreasing the polarization and leading to better electrochemical
105 performance. This result is confirmed by electrochemical impedance spectra of the samples (Fig. S4). Both of curves

compose a depressed semicircle in the region of high-to-medium frequencies and a sloping line in the region of low frequencies. The semicircle incarnates the charge-transfer resistance (Rct) between the electrolyte and the electrode. The sloping line is associated with the diffusion of lithium inside the electrode (Rw). Apparently, the porous Mn_2O_3 gives smaller Rct than microsized Mn_2O_3, implying better charge transfer kinetics. This result well explains the superior rate property and cycling stability of the porous Mn_2O_3 to the microsized Mn_2O_3.

In summary, hierarchically porous Mn_2O_3 are successfully synthesized using $[Mn(Br_4\text{-}bdc)(4,4'\text{-}bpy)(H_2O)_2]$ as a precursor. The resultant Mn_2O_3 displays the hierarchical porosity, which plays a significant role in the improvement of electrochemical properties. After 250 cycles at 1 A g^{-1}, the reversible capacity could be maintained at 705 mA h g^{-1}. To the best of our knowledge, this is one of the best performances of Mn_2O_3 based materials for LIBs. In the rate performance, hierarchically porous Mn_2O_3 exhibits a specific capacity of 450 mA h g^{-1} at 4 A g^{-1}, still higher than the theoretical capacity of commercial graphite. All the results suggest the promising potential of hierarchically porous Mn_2O_3 as advanced anode materials.

Acknowledgements

Notes and references

^{a} Research Institute of Surface Engineering, Taiyuan University of Technology, Taiyuan, 030024, China. Tel.: +86 351 6010540. E-mail: baizhongchao@tyut.edu.cn
^{b} A School of Chemistry and Chemical Engineering, Shandong University, Jinan 250100, China. Email: dsun@sdu.edu.cn.
†Electronic Supplementary Information (ESI) available: [the Experimental section, XRD pattern of Mn-LCP, SEM image of the microsized Mn_2O_3, TGA curve of the Mn-LPC and EIS of porous Mn_2O_3 and microsized Mn_2O_3.]. See DOI: 10.1039/b000000x/

1. V. Valtchev and L.Tosheva, *Chem. Rev.,* 2013, **113**, 6734.
2. Y. Wan and D.Y. Zhao, *Chem. Rev.,* 2007, **107**, 2821.
3. Z.C. Bai, B. Sun, N. Fan, Z.C. Ju, M.H. Li, L.Q. Xu, and Y.T. Qian, *Chem. Eur. J.,* 2012, **18**, 5319.
4. C. C. Yu, L. X. Zhang, J. L. Shi, J. J. Zhao, J. H. Gao, and D. S. Yan, *Adv. Funct. Mater.*, 2008, **18**, 1544.
5. Z.C. Bai, Z.C. Ju, C.L. Guo, Y.T. Qian, B. Tang and S.L. Xiong, *Nanoscale*, 2014, **6**, 3268
6. E. S. Toberer, T. D. Schladt and R. Seshadri, *J. Am. Chem. Soc.*, 2006, **128**, 1462.
7. B. Liu, X. Zhang, H. Shioyama, T. Mukai, T. Sakai and Q. Xu, *J. Power Sources*, 2010, **195**, 857.
8. C. Li, X. Yin, L. Chen, Q. Li and T. Wang, *Chem.-Eur. J.*, 2010, **16**, 5215.
9. L. Zhang, H.B. Wu, S. Madhavi, H. H. Hng and X.W. Lou, *J. Am. Chem. Soc.* 2012, **134**, 17388.
10. Y. C. Qiu, G. L. Xu, K.Y. Yan, H. Sun, J. W. Xiao, S. H. Yang, S. G. Sun, L. M. Jin and H. Deng, *J. Mater. Chem.*, 2011, **21**, 6346.
11. X. Zhang, Y.T. Qian, Y.C. Zhu and K.B. Tang, *Nanoscale*, 2014, **6**, 1725.
12. Y.J. Zhang, Y. Yan, X.Y. Wang, G. Li, D.R. Deng, L. Jiang, C.Y. Shu, and C.R. Wang, *Chem. Eur. J.*, 2014, **20**, 6126.
13. Y. Cai, S. Liu, X.M. Yin, Q.Y. Hao, M. Zhang and T.H.Wang, *Physica E*, 2010, **43**, 70.
14. Z.W. Chen, Z. Jiao, D.Y. Pan, Z. Li, M.H. Wu, C.H. Shek, C. M. L. Wu, and J. K.L. Lai, *Chem. Rev.*, 2012, **112**, 3833.
15. Y.F. Deng, Z.E. Li, Z.C. Shi, H. Xu, F. Peng and G.H. Chen, *RSC Adv.*, 2012, **2**, 4645.
16. C. Z. Yuan, H. B. Wu, Y. Xie and X. W. Lou, *Angew. Chem. Int. Ed.*, 2014, **53**, 1488.
17. D. Grosso, G.J. A.A. Soler-Illia, E.L. Crepaldi, B. Charleux and C. Sanchez, *Adv. Funct. Mater.*, 2003, **13**, 37.
18. Q. Liu, L.L. Yu, Y.Wang, Y.Z. Ji, J. Horvat, M.L. Cheng, X.Y. Jia,and G.X. Wang, *Inorg. Chem.*, 2013, **52**, 2817.
19. H. Kumagai, Y. Sakamoto, S. Kawata, .S. Matsunaga, and S. Inagaki, *Bull. Chem. Soc. Jpn.* 2012, **85**, 11021.
20. X. P. Fang, X. Lu, X. W. Guo, Y. Mao, Y. S. Hu, J. Z. Wang, Z. X. Wang, F. Wu, H. K. Liu and L. Q. Chen, *Electrochem. Commun.*, 2010, **12**, 1520.
21. Y. C. Qiu, G. L. Xu, K. Y. Yan, H. Sun, J. W. Xiao, S. H. Yang, S. G. Sun, L. M. Jin and H. Deng, *J. Mater. Chem.*, 2011, **21**, 6346.
22. J. Liu and D. F. Xue, *Adv. Mater.*, 2008, **20**, 2622.
23. Z.C. Bai, X.Y. Zhang, Y.W. Zhang, C.L. Guo and B. Tang, *J. Mater. Chem. A,* 2014, **2**, 16755.